Supporting Information

In Situ Quantification of Interactions between Charged Nanorods in a Predefined Potential Energy Landscape

Hoduk Cho,[1,2] Ivan A. Moreno-Hernandez,[1] Vida Jamali,[1] Myoung Hwan Oh,[3] and

A. Paul Alivisatos[1,2,4,5]*

[1]Department of Chemistry, University of California, Berkeley, CA, USA
[2]Materials Sciences Division, Lawrence Berkeley National Laboratory, Berkeley, CA, USA
[3]Chemical Sciences Division, Lawrence Berkeley National Laboratory, Berkeley, CA, USA
[4]Kavli Energy NanoScience Institute, Berkeley, CA, USA
[5]Department of Materials Science and Engineering, University of California, Berkeley, CA, USA
*e-mail: paul.alivisatos@berkeley.edu

Includes

Materials and Methods

Supplementary Figures

Supplementary Tables

Materials and Methods

Preparation of surface-functionalized lithographed nanorods

Nanorods were directly patterned on the 50 nm thick silicon nitride window of an E-chip (Protochips) using electron beam lithography. For creating a nanorod array that only consists of gold nanorods on 2 nm chromium, single-step lithography was sufficient as the corners of the silicon nitride window provided enough contrast to be utilized as alignment markers. For single-step lithography, E-chips were first washed with acetone and IPA to remove the protective resist coating. Then, they were plasma treated, spin-coated with 495-A2 PMMA (3000 rpm for 60 s), and baked on a hotplate at 185 °C for 5 min. Electron beam lithography was performed using a Crestec CABL-UH Series Electron Beam Lithography System (50 pA beam current and 130 kV acceleration voltage). After exposure, the patterns were developed in ice-cold 1:3 MIBK/IPA for 15 min and rinsed with IPA. Electron beam evaporation was used to deposit 2 nm of chromium adhesion layer and 10 nm of gold. Lift-off was achieved after immersing in Remover PG for 1 h at room temperature. PMMA, MIBK/IPA, and Remover PG were purchased from MicroChem. Nanorods in configuration A were 88.4±1.9 nm (length) by 11.7±0.5 nm (width) by 10.0±0.1 nm (thickness), with tip-to-tip and side-to-side spacings of 34 and 29 nm. In configuration B, nanorods were 89.8±2.0 nm by 12.7±0.5 nm by 10.0±0.1 nm, with tip-to-tip and side-to-side spacings of 33 and 150 nm.

For creating a nanorod array consisting of gold nanorods on 2 nm chromium and gold nanorods on 2 nm titanium, multistep lithography was required. For accurate registration, alignment markers were patterned first. Gold nanorods on titanium were then patterned with an intentional vacancy at the center of each 3 by 3 repeat unit, followed by the patterning of gold nanorods on chromium into these gaps. For multistep lithography, same fabrication procedures were used except that for the alignment markers (100 nm gold on 2 nm titanium), spin-coating was done with 950-A4 PMMA (2000 rpm for 60 s), electron beam lithography was performed at 2 nA, patterns were developed in MIBK/IPA for 1 min at room temperature, and lift-off was carried out with acetone (1h at room temperature). To compensate for the alignment error that is inherent to the instrument (~10 nm in horizontal and vertical directions), the arrays of gold nanorods on chromium were patterned with deliberate offsets (5 nm increments) in relation to the arrays of gold nanorods on titanium, ensuring that at least some regions of the final pattern will be well-aligned. Gold nanorods having dimensions of 87.5±2.8 nm by 12.9±1.0 nm by 10.0±0.1 nm were patterned on titanium with tip-to-tip and side-to-side spacings of 35 and 28 nm, while gold nanorods on chromium had dimensions of 65.7±8.3 nm by 16.5±1.3 nm by 10.0±0.1 nm.

To expedite the in situ lift-off of gold nanorods on chromium during liquid-phase TEM imaging, the chromium adhesion layer was partially etched by immersing the patterned E-chip in diluted CR-7 solution (Cyantek), with care being taken to avoid complete etching (which would result in ex situ lift-off). To functionalize the gold nanorod surface with carboxylic acid-terminated thioalkylated oligoethylene glycol ($HS\text{-}(CH_2)_{11}\text{-}(EG)_6\text{-}OCH_2\text{-}COOH$, Prochimia Surfaces), the patterned E-chip was plasma treated for a short time to remove any surface contaminants and then immersed overnight in 5 mM aqueous thiol solution inside a 1.5 mL centrifuge vial. Milli-Q water (18.2 MΩ at room temperature) was used throughout.

Although patterning on the smaller bottom E-chip (which is expected to provide better contrast and spatial resolution for liquid-phase TEM imaging) can be achieved by temporarily attaching it to a larger substrate, yield was higher for the larger top E-chip due to higher

reproducibility of the spin-coating step. We note that while nanofabrication was carried out on a chip by chip basis in this study, it can be scaled up by performing electron beam lithography on a partial/complete wafer of microchips before dicing into individual microchips.

TEM imaging

TEM imaging was performed at 200 kV on an FEI Tecnai T20 S-TWIN electron microscope equipped with a Gatan Orius SC200 CCD camera. Liquid-phase TEM experiments were carried out using a Poseidon 200 in situ liquid cell TEM flow holder. Top (EPT-52W) and bottom (EPB-52DF) E-chips, each with a 50 nm thick silicon nitride viewing window, were assembled with 1 μL of 5 mM thiol ligand solution. At the dose rate of 20 electrons $Å^{-2}$ s^{-1} used for data collection, gold nanorods on chromium did not detach simultaneously from the substrate. The stochastic nature of the lift-off process is attributed to the heterogeneous distribution of defects in the surface-passivating oxide layer of chromium, which is expected to affect the etching kinetics. When the dose rate was increased to 200 electrons $Å^{-2}$ s^{-1} or above, gold nanorods themselves were found to etch and disintegrate. Electron dose rate was calculated from the total pixel intensity by taking 10 counts to be equivalent to 1 electron. The frame rate used for video acquisition was 3.8 fps. Image processing and analysis were done using the Gatan Microscopy Suite software, ImageJ, and the MATLAB Image Processing Toolbox.

Nanorod tracking

The trajectory of the mobile central nanorod was obtained by image processing, which involved fitting the detected particle outline to an ellipse to identify its centroid and orientation and then imposing the projected shape of a spherocylinder of size equal to its dimensions measured at 0 s. Stationary nanorods surrounding the mobile central nanorod in the 3 by 3 array were approximated as equally sized spherocylinders, with their dimensions defined by the measured average dimensions of lithographed gold nanorods on titanium. The positions of surrounding stationary nanorods were determined based on the measured center position of the 3 by 3 array and the measured average inter-rod spacings of lithographed gold nanorods on titanium.

Theoretical modeling of nanorod interactions

Modeling of the 3 by 3 array of charged nanorods was performed by constructing three-dimensional surfaces of spherocylinders using evenly spaced simulation points (0.033 simulation points per nm^2). Since the negatively charged ligand headgroups are responsible for the electrostatic repulsion, experimentally measured average nanorod dimensions were adjusted to account for the ligand shell thickness of 2.4 nm (Table S1).[1] Pairwise summation of screened electrostatic repulsion between point i on the central nanorod and point j on a surrounding nanorod is given by the following equation[2]:

$$U_{elec} = \sum_{i,j} \frac{z^2 e^2}{4\pi\epsilon_0\epsilon_r r_{ij}} \exp\left(-\frac{r_{ij}}{\lambda_D}\right) \quad (1)$$

where U_{elec} is the electrostatic component of the interaction energy, z is the number of

charges per simulation point, e is the elementary charge, ϵ_0 is the vacuum permittivity, ϵ_r is the relative permittivity, r_{ij} is the distance between the two points, and λ_{D} is the Debye screening length. Surface charge density, σ, is simply the total charge on the nanorod (z x e x number of simulation points) divided by the total nanorod surface area. By translating and rotating the central nanorod, we computed the potential energy for all possible configurations.

The relationship between the probability of finding a particle at a certain position, $p(x,y)$, and its corresponding potential energy, $U(x,y)$, is described by the Boltzmann distribution:

$$p(x,y) \propto \exp\left(-\frac{U(x,y)}{k_{\mathrm{B}}T}\right) \tag{2}$$

where k_{B} is the Boltzmann constant and T is the temperature. Equation (2) was used to convert the theoretical potential energy map into the corresponding probability distribution of centroid positions. Before fitting, both experimental and theoretical probability distributions of centroid positions were normalized by dividing by the highest probability value. Surface fitting was carried out by aligning the peak positions and minimizing the mean squared error, which yielded λ_{D} and σ values of 18.6 nm and -7.85 mC m^{-2}.

To model the energetics of translational tip-to-tip, rotational tip-to-tip, and side-to-side attachment pathways for a pair of charged nanorods, we first generated idealized attachment trajectories by linearly interpolating between the initial unassembled and final assembled states that correspond to each attachment mode, in terms of both spatial and angular coordinates of nanorods involved (Table S2). We then calculated the total interaction energy as the pair of nanorods approached each other in incremental steps. For calculating U_{elec}, the pairwise summation procedure was carried out for two spherocylinders of radius 8.4 nm and length 92.8 nm (0.44 simulation points per nm^2), using values of 18.6 nm and -7.85 mC m^{-2} for λ_{D} and σ. The van der Waals component of the interaction energy, U_{vdW}, for translational and rotational tip-to-tip attachment pathways was calculated by modeling it as the interaction between two spheres that represent the nearest tip regions of the nanorods. This was justified by the fact that U_{vdW} is only significant at small interparticle distances. For two spheres of radius R that are separated by distance D, U_{vdW} is given by the following equation[2]:

$$U_{vdW} = -\frac{A \cdot R}{12D} \tag{3}$$

where A is the Hamaker constant (2.5 x 10^{-19} J for gold[3]). For side-to-side attachment, U_{vdW} was calculated by modeling the nanorods as cylinders. For two parallel cylinders of radius R and length L that are separated by distance D, U_{vdW} is given by the following equation[2]:

$$U_{vdW} = -\frac{A \cdot L\sqrt{R}}{24D^{3/2}} \tag{4}$$

MATLAB codes used for modeling nanorod interactions are freely available from GitHub (https://github.com/AliviGitHub).

Supplementary Figures

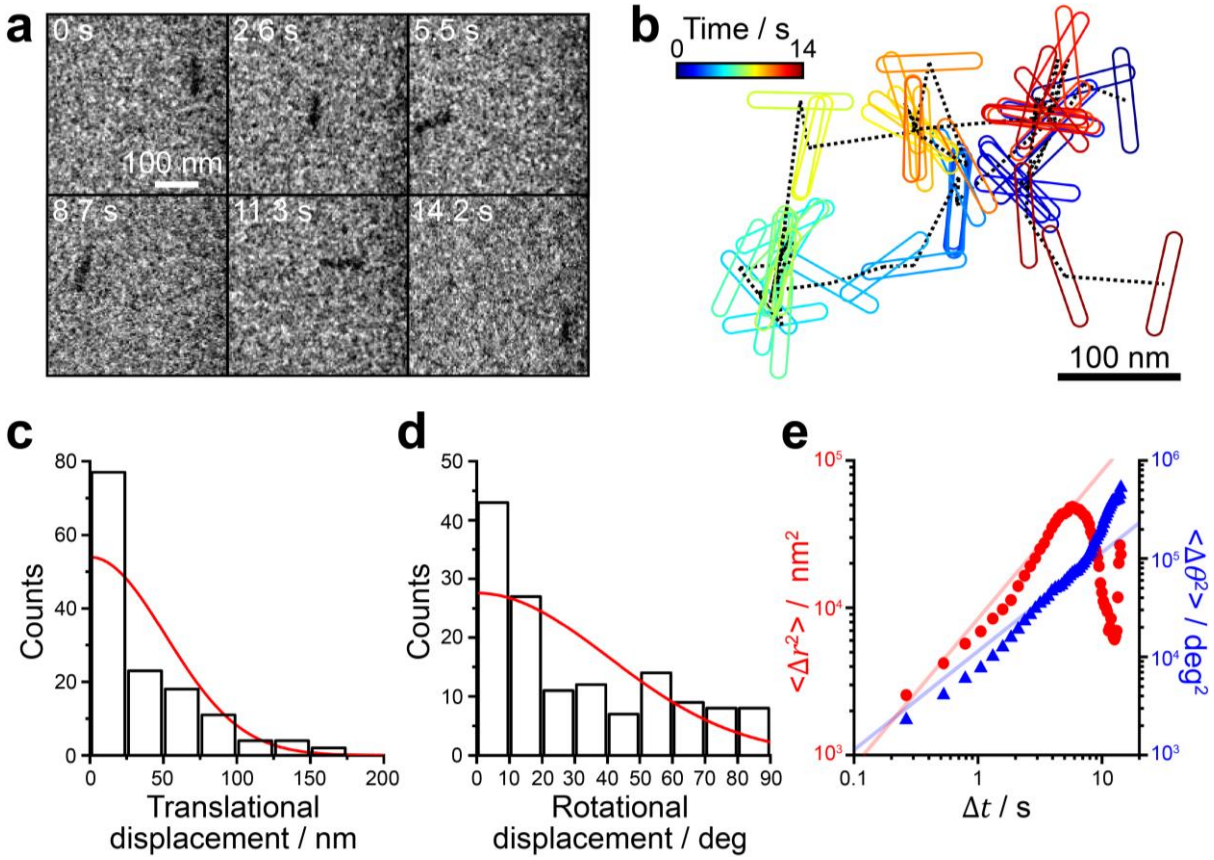

Figure S1. Brownian motion of a free nanorod following lift-off. (a) Time series of TEM images showing the dynamics of a free nanorod after lift-off. (b) Trajectory of the nanorod in (a). (c) Distribution of absolute translational displacements overlaid with a Gaussian fit. (d) Distribution of absolute rotational displacements overlaid with a Gaussian fit. (e) Translational mean squared displacement ($<\Delta r^2>$) and angular mean squared displacement ($<\Delta\theta^2>$) versus time interval (Δt).

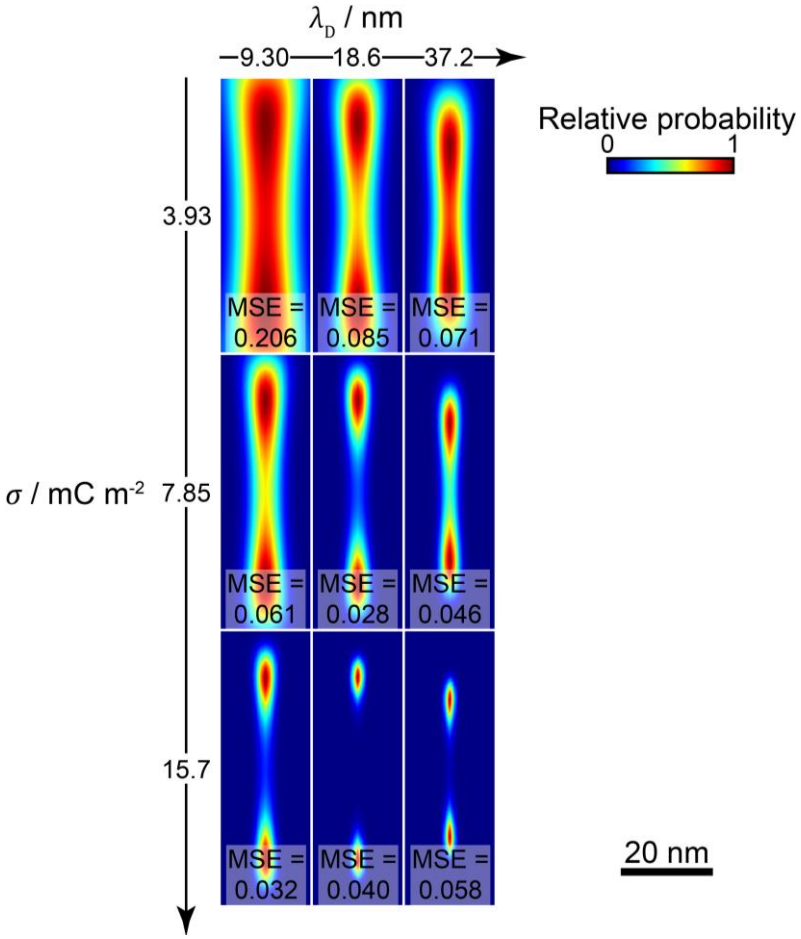

Figure S2. Probability distributions of centroid positions generated using different values for the Debye screening length (λ_D) and the surface charge density (σ) are displayed with their corresponding mean squared error (MSE) values. Fitting was done by minimizing the MSE.

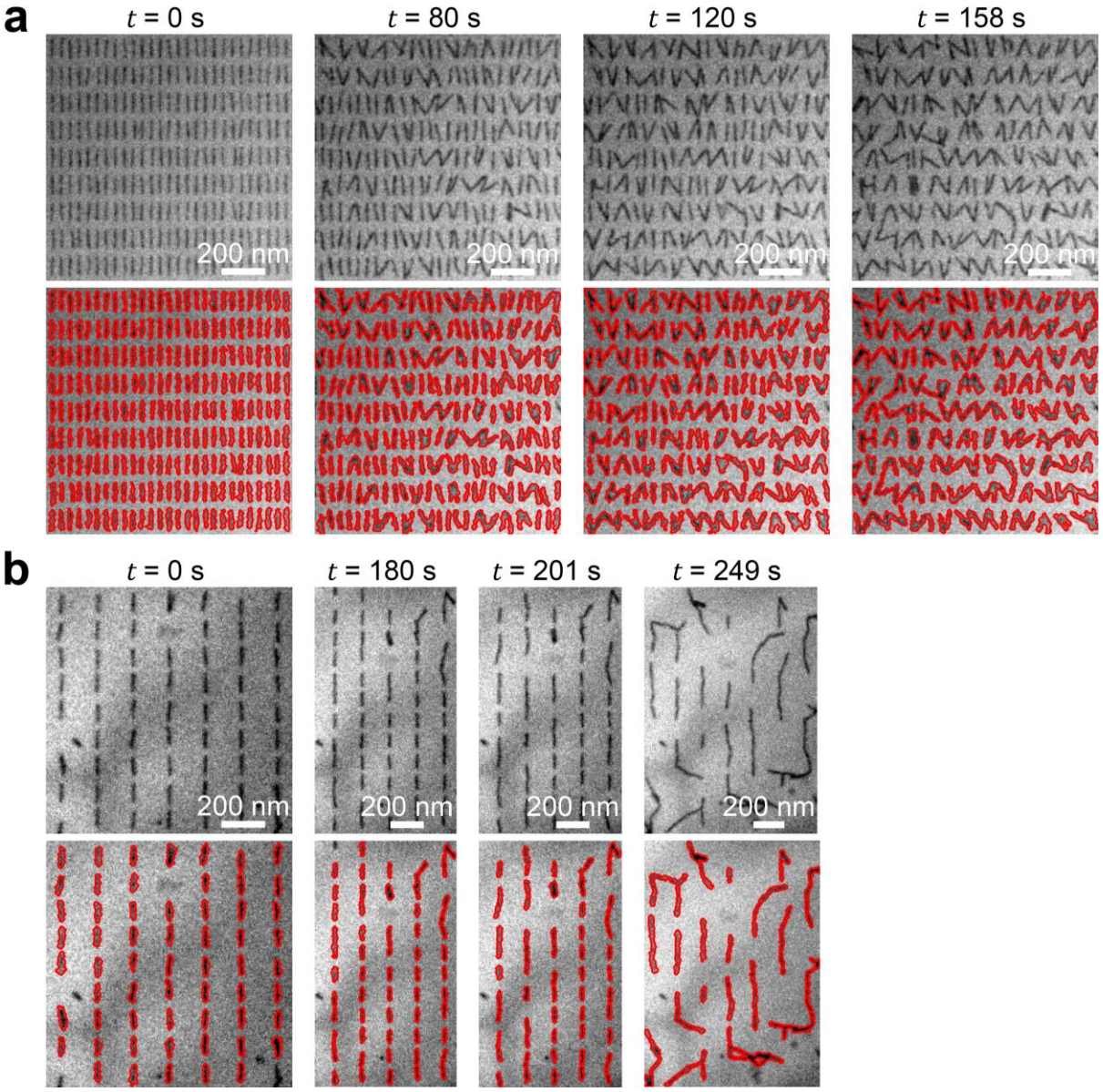

Figure S3. Quantitative image analysis for characterizing nanorod assemblies. Raw and processed TEM images for configurations A (a) and B (b) at the specified times (t). The projected area and the maximum caliper length (or equivalently, the maximum Feret diameter) were measured for individual nanorods and nanorod assemblies.

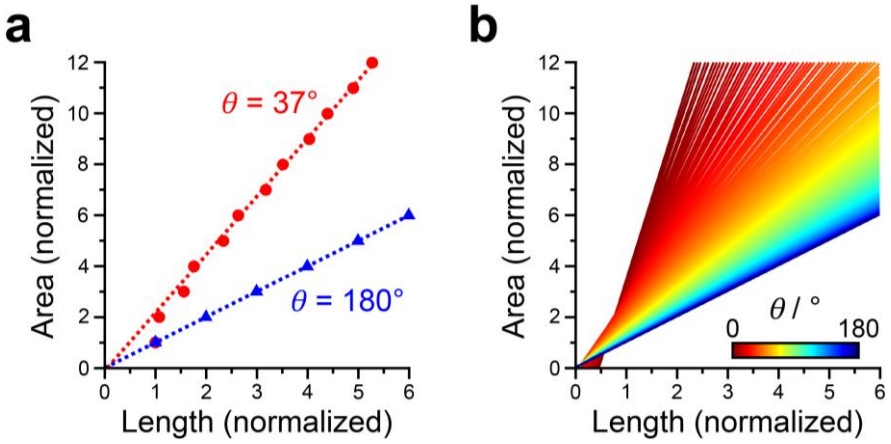

Figure S4. Predicted trend lines for idealized nanorod assemblies. (a) Trend lines were obtained by linearly fitting the data points calculated for different lengths of idealized nanorod assemblies with a fixed attachment angle. Assuming no overlap of ligands, the nanorod length and width were set as 92.8 and 16.8 nm, resulting in an aspect ratio of 5.5. The data points for nanorod assemblies containing more than 6 nanorods rapidly converged to a straight line. (b) Trend lines obtained for the entire range of possible attachment angles.

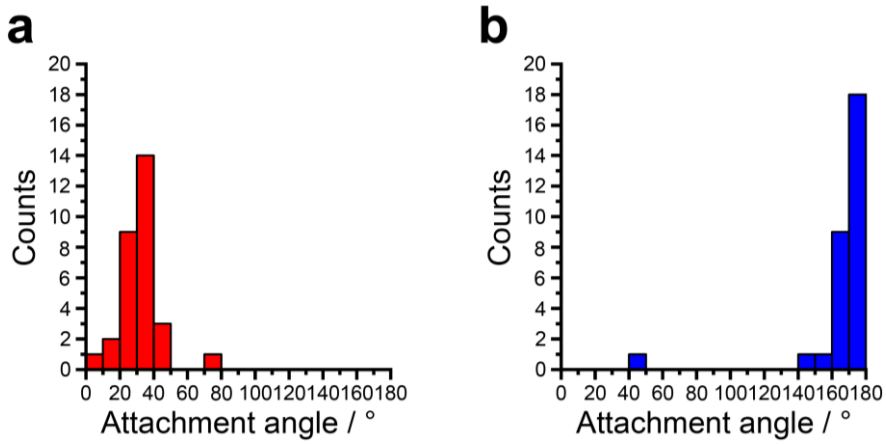

Figure S5. Distribution of attachment angles for nanorod dimers. Attachment angles for individual nanorods coming together to form dimers were measured for configurations A (a) and B (b). For each configuration, 30 dimers were analyzed.

Supplementary Tables

Table S1. Construction of the 3 by 3 array of nanorods.

	Coordinates [nm, nm, °]	Radius (nm)	Length (nm)
Rod 1	[-41, 122, 0]	8.4	92.8
Rod 2	[0, 122, 0]	8.4	92.8
Rod 3	[41, 122, 0]	8.4	92.8
Rod 4	[-41, 0, 0]	8.4	92.8
Rod 5	[X, Y, θ]	10.4	70.8
Rod 6	[41, 0, 0]	8.4	92.8
Rod 7	[-41, -122, 0]	8.4	92.8
Rod 8	[0, -122, 0]	8.4	92.8
Rod 9	[41, -122, 0]	8.4	92.8

Table S2. Initial and final states for different attachment trajectories.

		Initial coordinates [nm, nm, °]		Final coordinates [nm, nm, °]
		Config A	Config B	
Translational tip-to-tip	**Rod 1**	[0, 0, 0]	[0, 0, 0]	[0, 0, 0]
	Rod 2	[0, 122, 0]	[0, 122, 0]	[0, 92.8, 0]
Rotational tip-to-tip	**Rod 1**	[0, 0, 0]	[0, 0, 0]	[0, 0, 18.5]
	Rod 2	[41, 0, 0]	[162, 0, 0]	[41, 0, -18.5]
Side-to-side	**Rod 1**	[0, 0, 0]	[0, 0, 0]	[0, 0, 0]
	Rod 2	[41, 0, 0]	[162, 0, 0]	[16.8, 0, 0]

References

(1) Jones, M. R.; Macfarlane, R. J.; Prigodich, A. E.; Patel, P. C.; Mirkin, C. A. Nanoparticle Shape Anisotropy Dictates the Collective Behavior of Surface-Bound Ligands. *J. Am. Chem. Soc.* **2011**, *133*, 18865-18869.
(2) Israelachvili, J. N. *Intermolecular and Surface Forces*; Academic Press, 2011.
(3) Biggs, S.; Mulvaney, P. Measurement of the Forces between Gold Surfaces in Water by Atomic Force Microscopy. *J. Chem. Phys.* **1994**, *100*, 8501-8505.